Vision guided learning based bimanual robot sewing

Bidan Huang, Alessandro Vandini, Yang Hu, Guang-Zhong Yang, *Fellow, IEEE*

***Abstract*—**

I. Introduction

Sewing is a delicate and pain-stacking task. Recent development in robotics has largely increased the efficiency of the sewing industry. Most of these robotic solutions are specialised in one or a few certain types of machine stitches, such as the lock stitches. Some conventional hand stitches are hard to automate and still requires human labour. Our motivation of the study is to free human from the tiring sewing jobs and teach the robot to make hand stitches. Particularly, we focus on the task of personalized stent graft manufacturing.

A stent graft is a tubular structure composed of fabric supported by a metal mesh called stent. It is widely used for a variety of pathologies during endovascular interventions, such as reinforcing the vessel wall in presence of aneurysms. Clinically, each stent graft needs to be customised to the patient anatomy, with fenestrations (openings) on the graft body to maintain the patency of side branches to vital organs. They often come at a significant cost in addition to a long manufacturing process. This is mainly due to the intensive manual tasks involved in the process. As a consequence, patients are more likely to be subjected of complications, e.g. aneurysm eruption, during the waiting period and precluding treatment to patients presenting acutely. Improved manufacturing of personalised stent grafts is therefore a critical unmet clinical demand and we are pursuing a robot assisted manufacturing approach. This study focuses on the key process of the stent graft manufacturing: sewing the stent to a fabric tube. For this purpose, a robotic system is proposed here in order to replicate the hand stitches required during the stent graft manufacturing process.

Automated sewing has been extensively researched in textile industry. Intelligent robotic systems with multi-sensor feedback are built to work in conjunction with a traditional sewing machine. Important topics in this filed includes bimanual robotic sewing [7], fabric tension control, and seam tracking [14], [15]. To cope with environmental changes during the sewing process, various control strategies are implemented, such as a fuzzy logic controller [6], a hybrid position/force control [7], a leader/follower control strategy [13]. In addition, extensive research has been carried out in the design of sewing heads capable of access the sewn object from a single side, which allows the sewing to be performed on a 3D surface. For example, KSL Keilmann (Lorsch, Germany) [6] has develop various 3D stitching systems incorporating single sided sewing heads onto KUKA manipulators for sewing fabric-reinforced structure of aircraft parts. These machines are designed for sewing large and heavy objects. Delicate sewing for small objects with non uniform shapes are still mainly hand made.

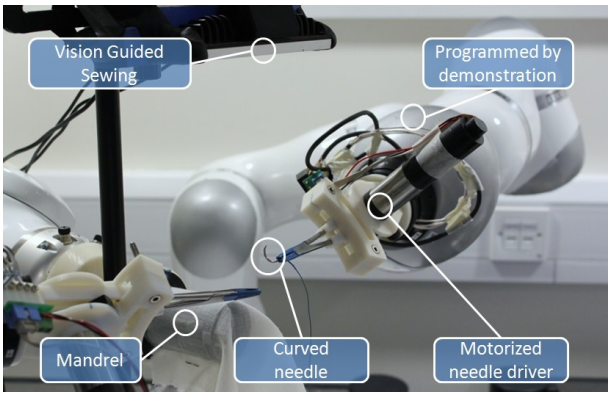

Fig. 1: Robot sewing system for personalized stent graft manufacturing

As the emerging of robotic assisted systems in the field of minimally invasive surgery, research on automated suturing tasks is also widely investigated, which provides the advantage of the machine speed and accuracy of the suturing process. A suturing task can be divided into two sub-tasks: tissue piercing and knot tying. For each task, research is carried by planning the procedure according to well established manual suture techniques [4], [5], [11] or learning the skills from expert demonstrations [10], [12], [17]. Vision guidance/visual servoing plays a key role in the achievement of a fully automated suturing task. In the aspect of positioning the needle to the target point, both the needle posture and the target suturing plane posture need to be measured. Iyer et al. [3] proposed a single arm single camera system auto-suturing system in which the area being sutured on is marked by round markers. In their method, the monocular pose measurement algorithm [9] was used for estimating the needle posture. Another work presented by Staub et al. [16] introduced 3D stereo system and visual servoing technique to improve the accuracy in aligning the needle with target stitching point. Recently, an auto-suturing system with 2D camera guidance and motorized Endo 360 suturing device is presented [8]. In this work, a method is presented to track incision contour and automatically distributes equally-spaced stitches along the incision.

B. Huang, A. Vandini, Y. Hu and G.-Z. Yang are with the Hamlyn Centre for Robotic Surgery, Imperial College London, SW7 2AZ, London, UK (e-mail: b.huang@imperial.ac.uk). Bidan Huang and Yang Hu was supported by the EPSRC (EP/L020688/1).

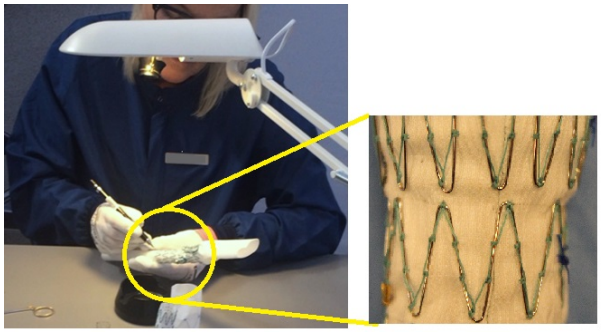

Fig. 2: A lady is hand sewing stent graft.

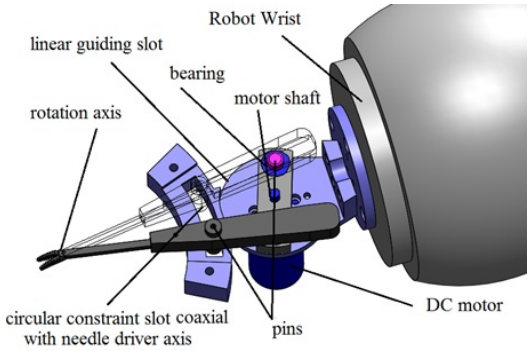

Fig. 3: Motorized needle driver

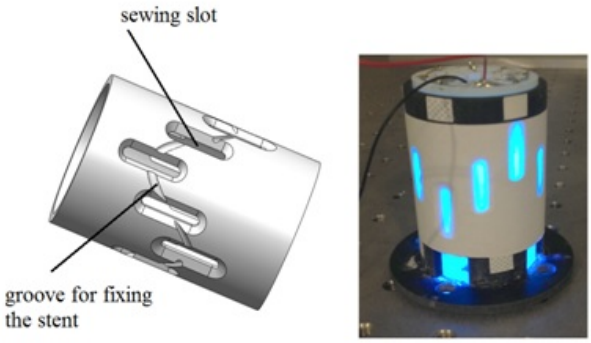

Fig. 4: Mandrel

Inspired by these medical sewing approaches, we use robots to control a needle driver to manipulate a curved needle for sewing. Compare to conventional sewing machines, this approach is more versatile, allowing us to do stent sewing, fenestration finishing and knot tying with the same setup. A learning from human demonstration approach is used here so that the robot sewing movements can be programmed easily.

The use of curve needle also gives us the benefit of doing single sided sewing. The shape of the fabric tube, i.e. the graft, is pre-designed for the patient anatomy and pre-manufactured. The tube can not be flattened into a single layer and hence conventional techniques of sewing a flat fabric is not applicable. Single sided sewing is an effective solution. Inspired by the conventional method of sewing stent grafts, we design a mandrel to support the fabric from the inside (Figure **??**). Figure 1 shows our sewing system. To ensure the stitch quality and the system robustness, we use a vision system to guide the sewing process. As far as we know, this is the first automotive sewing system that use curved needle to make hand stitches.

This paper presents the proposed system and is organized as follows. Section 2 describe our system, both the hardware design and the software components. Section 3 shows the experiments we conduct using this system and presnets the results, followed by the discussion in Section 4.

II. System Overview

This section describes our system for robot sewing with a curved needle. Our system is consisted with two Kuka 7 d.o.f robots: one robot to manipulate the needle, i.e. piercing and one to control the fabric tube. The robot manipulating the needle is mounted with a motorized needle driver and the one controlling the fabric is mounted with a mandrel. This mandrel is placed inside the fabric tube to bound it tightly with the stent (Figure **??**). To ensure the the stent graft quality, each stitch is required to be at the correct place and have the correct length. We use a vision system to guide the robot movements in order to maintain the accuracy. The needle position is tracked during the whole task. The robot movements are first learned from human hand stitch demonstrations and then regenerated online to deliver the needle to stitch at the correct spot.

A. Hardware design

A surgical curved needle is used in our task to perform sewing (Figure 1). It is manipulated by a surgical needle driver. This needle driver is widely used in laparoscopic surgery and is specially designed to hold firmly the needle. In our system, the needle driver is motorized for the robot to drive it (Figure **??**). This design has two set of constraints/guiding slots working in conjunction with pins. The linear slot lies in the direction along the handle of the needle driver and the constraint slot is coaxial with the needle driver axis; therefore the motor rotation can be mapped to the open and close of the needle driver. To reduce frictions in driving this mechanism, bears are used. All the mechanical components are 3D printed.

Our mandrel is a 3D printed hollow cylinder to support the fabric. Its outer surface has groove for fixing stent and it supports the stent to tightly attache with the fabric. Slots are opened on the mandrel at the positions of stitches. They allow the needle to pierce in and out and hence sewing the stent on the fabric. An additional function of the slots is location marker: when illuminated from inside the mandrel, the location of the slots are visible, allowing us to identify the exact sewing positions.

B. Learning from human demonstration

With the current state of art, personalized stent grafts are hand sewn. This is because the delicate control of the needle is hard to programm to robotize. To tackle this problem, we adopt an learning for human demonstration approach

for this task. Our learning starts by demonstrating to the robot multiple times how to make a stitch. The demonstrated motions are then segmented to three phases. A Gaussian Mixture Model (GMM) [2] is used to encode each phases of the sewing motion and the generalised motion is then retrieved via Gaussian Mixture Regression (GMR). Generally speaking, this learning process involves the following steps:

1) 1: Human demonstration of sewing
2) 2: Motion segmentation
3) 3: Primitive motions learning

1) Human demonstration of sewing: The first step is to recode the stitching motion from human demonstrations. Human single side hand sewing motion involves a couple of stages including 1) needle approaching fabric, 2) needle piercing in, 3) releasing needle root 4)griping the needle tip and 5) pulling the needle out, 6) passing the needle to another hand and 7) picking up the needle head. At the beginning of the task, the needle driver grip firming the needle root. When the tip of the curved needle pierces out from the bottom of the fabric, the needle driver release the needle. The needle is remained in the same pose by the friction of the fabric. The needle driver is then approach the tip of the needle, and grip the tip. The needle then being pulled out from the fabric. Once the needle is completely pulled out from the fabric, the needle driver pass it to another fixed needle driver to re-grip the needle head. After re-griping, the needle driver move back to the starting position and finish a full circle of one stitch.

We use the kinesthetic teaching method to demonstrate all these stages to the robot. The robot is put in gravity compensation mode and its movement is guided by human. The needle driver open and close is controlled an electronic footpedal. The movement of the robot, as well as the needle driver status, i.e. open and close, are recorded. During the demonstrations, when the needle driver is close, we assume the needle is firmly connected with the driver and hence no slip between the needle and the driver will occur. Hence, during the demonstrations, we presume the relative pose between the needle and the driver is a constant value. All the trajectories are recorded in 6 d.o.f with euler angles $\{\alpha,\beta,\theta\}$ representation of the orientation and $\{x,y,z\}$ representing the robot end effector position. The needle position is computed from the end effector position.

During the needle piercing, we take an object centric approach of learning. This is to say, we learn the motion of the object, i.e. the needle, rather than the movement of the robot. This object centric approach allow us to generate adaptive robot motions to perform the same stitch under different conditions, such as different needle poses. In our task, the needle movements for each stitch should the exactly the same so that the quality of the sewing is maintained. When the robot release the needle, we learn the robot movements so that it approaches the needle tip in a proper pose to grip it. To this end, we segment the stitch motions to three phases. The next section details our segmentation method.

2) Motion segmentation: With all the collected training data (sewing trajectories), we segment each trajectory to reflect the different stages of sewing and learn each stage independently. This segmentation is done based on the relation between the needle and its driver: attached or detached. When the needle is attached to the driver, we take the object centric approach and learn the needle movement so that the needle can repeat the same movement every time. When the needle is detach to the driver, we focus on learning the needle driver trajectory in order to reach the proper location to grip the needle.

Therefore, we use the needle driver open and close events to segment the trajectories (Figure 6). Each segment is then learned as a primitive movement and encoded by a statistical model.

Before learning models for each primitive movements, we apply the Dynamic Time Warping (DTW) [1] to align the data across different demonstrations. DTW is a technique that temporally warps the data and find the best match between two time series according to their key features. In our task, velocity variations do not effect the task quality and hence DTW does not effect our training data.

3) Primitive motion learning: After the we segments the data to a set of primitive movements, we build a model *Omega* to encode each primitive. The same primitive of different trails of the demonstrations are put together as the training data. Each primitive is represented in seven dimension: one temporal value $\{t\}$, three spatial values $h=\{x,y,z\}$ and three orientation values $o=\{\alpha,\beta,\theta\}$. A joint distribution $p\{t,h,o \mid \Omega\}$ is builded by using *GMM*. We choose to use *GMM* because of it's capability of encoding non-linear data and it's robustness of extracting constrains from noise data.

With N Gaussian components, the joint distribution is represented as:

$$\begin{aligned} p(t,h,o \mid \Omega) &= \sum_{n=1}^{N} \pi_n p(t,h,o \mid \mu_n,\Sigma_n) \\ &= \sum_{n=1}^{N} \pi_n \frac{1}{\sqrt{(2\pi)^D \mid \Sigma_n \mid}} e^{-\frac{1}{2}(\{t,h,o\}-\mu_n)^\top \Sigma_n^{-1}(\{t,h,o\}-\mu_n)} \end{aligned} \tag{1}$$

where π_n is the prior of the n^{th} Gaussian component, D the number of variables, and the μ_n, Σ_n the corresponding mean and covariance. For the n^{th} Gaussian component, the mean and covariance μ_n, Σ_n is:

$$\boldsymbol{\mu}_n = \begin{pmatrix} \boldsymbol{\mu}_{t,n} \\ \boldsymbol{\mu}_{h,n} \\ \boldsymbol{\mu}_{o,n} \end{pmatrix} \qquad \boldsymbol{\Sigma}_n = \begin{pmatrix} \boldsymbol{\Sigma}_{tt,n} & \boldsymbol{\Sigma}_{th,n} & \boldsymbol{\Sigma}_{to,n} \\ \boldsymbol{\Sigma}_{ht,n} & \boldsymbol{\Sigma}_{hh,n} & \boldsymbol{\Sigma}_{ho,n} \\ \boldsymbol{\Sigma}_{ot,n} & \boldsymbol{\Sigma}_{oh,n} & \boldsymbol{\Sigma}_{oo,n} \end{pmatrix} \tag{2}$$

Each primitive movement is encoded by one model. A smooth generalized trajectory satisfying the constraints encoded with the *GMM* is extracted by using the Gaussian Mixture Regression (GMR). With the $i-th$ primitive movement model Ω_i, we use a temporal value t to query the trajectory

$\{h,o\}$. Here we define:

$$\mu_n = \begin{pmatrix} \mu_n^t \\ \mu_n^{ho} \end{pmatrix} \qquad \Sigma_n = \begin{pmatrix} \Sigma_n^{tt} & \Sigma_n^{t,ho} \\ \Sigma_n^{ho,t} & \Sigma_n^{ho,ho} \end{pmatrix} \tag{3}$$

The *GMR* estimate the conditional expectation value as $\hat{\mu}_{ho}$ with variance $\hat{\Sigma}_{ho}$:

$$\hat{\mu}^{ho} = \sum_{n=1}^{N} \beta_n \hat{\mu}_n \qquad \hat{\Sigma}^{ho,ho} = \sum_{n=1}^{N} {\beta_n}^2 \hat{\Sigma}_n \tag{4}$$

where

$$\hat{\mu}_n = \mu_n^{ho} + \Sigma_n^{ho,t} (\Sigma_n^{tt})^{-1} (t - \mu_n^{ho}) \tag{5}$$

$$\hat{\Sigma}_n = \Sigma_n^{ho,ho} - \Sigma_n^{ho,t} (\Sigma_n^{tt})^{-1} \Sigma_n^{t,ho} \tag{6}$$

and

$$\beta_n = \frac{\pi_n p(t|\mu_n^t, \Sigma_n^{tt})}{\sum_{n=1}^{N} \pi_n p(t|\mu_n^t, \Sigma_n^{tt})} \tag{7}$$

C. Vision System

The vision system is a key part to maintain the our stitch quality. During the sewing task, defect can occur by the slippage of the needle on the needle drivers. This usually happens during the passing stage: when one robot passes the needle to another, small displacements of the optimal relative pose between the needle and the needle driver can occur. We use a stereo vision system to monitor the process and measure the displacements. Adaptive robot movements are then generated to cope with these small displacements and deliver the needle to the target.

First, the needle is detected in each stereo image using the needle detection algorithm proposed in [**?**]. For this purpose, a feature image, i.e. I_H, based on the analysis of the eigenvalues of the Hessian matrix [**?**] is computed to enhance curvilinear structure in the image. Assuming that a calibrated imaging system is available, the 3D points of the needle defined by its *ideal* pose are projected in the image plane. This is performed in order to include a prior information of needle's shape in the detection algorithm. Although the *ideal* pose of the needle is usually different from its real one due to slippage, it still represents of a good guess of the needle pose. Thus, small straight segments are detected in I_H, and only segments that are close to the projected needle and have similar orientation are considered as needle's parts. Finally, these segments are combined in order to create a continuous curve that represents the detected needle in the images. To improve the detection of the needle, the needle driver is also detected in the images using color-base segmentation in HSV space. This allows the reduction of false positive detections of needle segments which are mainly caused by the presence of the needle driver.

The 3D reconstruction of the needle is performed by triangulating the detected needle points of the stereo image pairs. In the current setup, a section of the needle is occluded, however, in the images due to the presence of the needle driver. To overcome the occlusion and to estimate the new needle pose a discretization of the reconstructed needle and the needle defined by the *ideal* position is performed. Starting from the needle tip, points are sampled along the needle shape at distance equal to the arch length of 1 millimetre generating a set of equidistant 3D points, defined by N_{ide} for the ideal and N_{est} for the reconstructed needle, respectively. Finally, a rigid transformation that best maps the two set of points N_{ide} and N_{est}, i.e. the *new* needle pose, is calculated using singular vector decomposition (SVD).

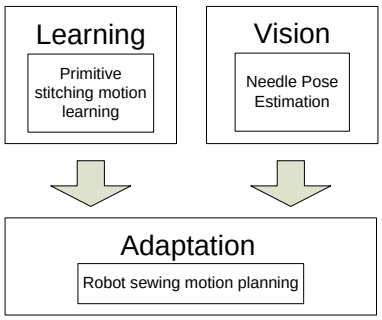

Fig. 5: System overview of stent graft sewing system. The robot is programmed by demonstrations. During task execution, the vision system estimate the needle pose and hence compute an adaptive trajectory for the sewing movements

D. Task execution

The relative posture between the needle driver and the needle may change during task execution. This situation happen frequently during needle regrasping procedure, in which the needle may not in its original place during demonstration. To keep the learned needle trajectory and perform fabric piercing precisely, the robot end-effector trajectory needs to be modified in order to adapt to the new needle posture, so each time before performing fabric piercing, needle pose estimation is performed using the stereo vision system and the relative transformation between the ideal needle posture and actual needle posture is calculated. Using the hand-eye calibration matrix, a new robot end-effector trajectory can be achieved.

III. Experiments

A. System setup

A system with two articulated KUKA Lightweight-4 robots is built (Figure **??**): one robot is mounted with a motorized needle driver holding a curved needle, the second robot holds a mandrel with a stent graft. The mandrel, shown in Fig 2, is a cylinder with grooves for fixing the stent and is characterized by the presence of slots to allow the sewing. The sewing process is as below:

1) Needle driver holding the end point of the needle
2) Vision system detects the needle pose relative to the needle driver
3) New robot trajectory is generated according to the needle pose
4) Needle driver approaching mandrel
5) Needle piercing into the fabric and the tip piercing out of fabric
6) Needle driver releasing the end point of the needle, approaching the needle tip

7) Needle driver griping the needle tip and pulling out the needle out of fabric
8) Needle driver bringing the needle to the second needle driver
9) The second needle driver griping the middle of the needle, the first needle driver griping the end point of the needle

The stereo system is consisted of two Logitech C930E cameras. Stereo calibration is performed by using OpenCV library. The calibration accuracy is measured by using the triangulation results to measure distance between two feature points on the camera view. The error is 0.89 *mm*.

The camera frame is registered to the robot frame by hand-eye calibration. During the calibration, a key dot pattern is fixed on a know position of the robot end effector, whose origin is aligned with the end effector origin. The robot moves the key dots around and records the end key dot pattern positions in the robot frame, as well as in the camera frame. The rigid transformation between these two set of positions are computed by using the singular value decomposition technique. This transformation is hence the transformation from the robot frame to the camera frame. We mount the motorized needle driver on the end effector and register the tip pose to the robot. With the result of the hand eye calibration, the needle driver pose in the camera frame is computed.

The needle is initially grip at the very end of the needle driver and we assume that only small displacement of the needle pose will occur during the sewing task. The needle driver tip position is hence used as a prior of the needle position.

B. Learning

For teaching robot the sewing task, we carry out four demonstrations. All demonstrations starts from the same position and sew the same slot on the mandrel. To control the quality of the stitches, across all demonstrations the needle pierces in at the same location and pierces out at the same location. At the beginning of each demonstration, the needle is placed at the same place and normal to the needle driver.

The demonstrations are segmented into three primitive movements, according to the needle drive open and close even. Figure 6 shows one segmentation results. Figure 8 shows the demonstrated needle driver trajectories in 3D.

GMM is used to learn model for each phase. Figure **??** shows a 2D projection of the build model of each phase. It can be seen from the model that the three phases have different characteristics. Phase one has small variance from the beginning to the end, as all the movements start from the same point and pierce into the same location. The piercing movements are the same in order to produce similar stitches. Phase two has larger variance compare to phase one, as the needle is detached with the robot and the robot movement has less constraints. Phase three has small variance at the beginning, when the robot needs to pull out the needle from the same location, and has large variance once the needle is pulled out from the fabric. These show that the GMM can effectively capture the constraints at each phase and hence generate proper trajectories for the robot to complete the task.

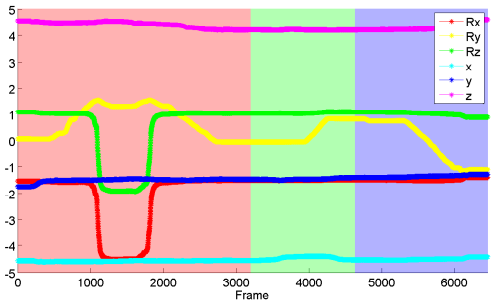

Fig. 6: Segmentation result of human demonstration. The red, green and blue patches label the three segments of the motion

C. Vision for needle pose estimation

Extensive evaluation of the needle reconstruction algorithm is performed by estimating the 3D needle reconstruction error. This metric measures the distance between the reconstructed 3D shape of the needle and the ground truth shape. The ground truth is generated by segmenting manually the positions of the needle in each stereo image which are then used to find the ground truth 3D needle shape by triangulation. The 3D needle reconstruction error, i.e. $Dist(N_{gt}, N_{est})$, between the estimated needle, N_{est}, with respect to the ground truth shape, N_{gt}, is defined as:

$$Dist(N_{gt}, N_{est}) = \frac{1}{w+f}\left(\sum_{i=1}^{w} d_{min}(N_{gt}(i), N_{est}) + \sum_{j=1}^{f} d_{min}(N_{est}(j), N_{gt})\right) \quad (8)$$

where w and f are the cardinality of the set of points of N_{gt} and N_{est}, respectively, and $d_{min}(N_{gt}(i), N_{est})$ is the Euclidean distance between the i^{th} point of N_{gt} to the closest point on N_{est}. The distance *Dist* is also presented in [**?**]. The mean and standard deviation of the 3D needle reconstruction error for the experiment is 0.512 ± 0.097 millimetres. Thus, the needle reconstruction reaches sub-millimetres accuracy allowing a robust needle pose estimations which intrinsically depend on the needle reconstruction.

D. Task execution

Before starting replay the learned trajectory, needle posture detection is performed and the transformation between the new needle posture and the ideal needle posture is calculated. Then a new needle driver trajectory is generated according to the transformation. if the needle posture is different with the one presented in demonstration, then the robot needs to adapt a new posture in order to pierce the fabric as the same way it did in the demonstration. As soon as the needle tip comes from the fabric, the needle is released and it stay in the fabric. The robots then goes to grasp the needle tip and takes it out from the fabric. Due to the deformation of the fabric, the needle cannot be kept in a good posture for regrasping.

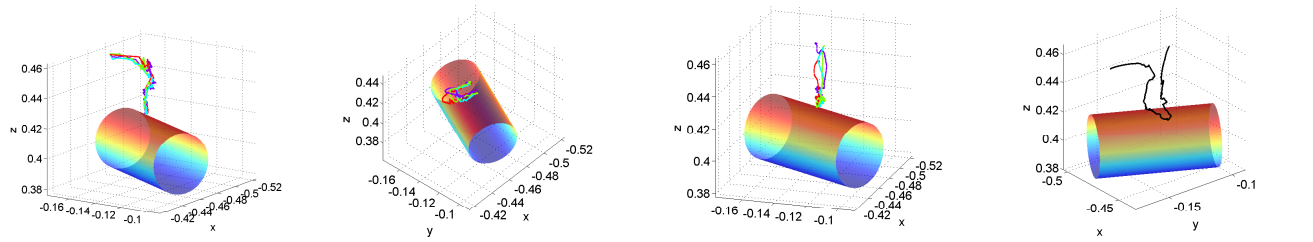

(a) Demonstrations of phase 1 (b) Demonstrations of phase 2 (c) Demonstrations of phase 3 (d) Learnt trajectory of phase 1,2 and 3

Fig. 7: Needle driver trajectories of human demonstrations and the learnt result. Each color represents one demonstration. The cylinder represents the mandrel

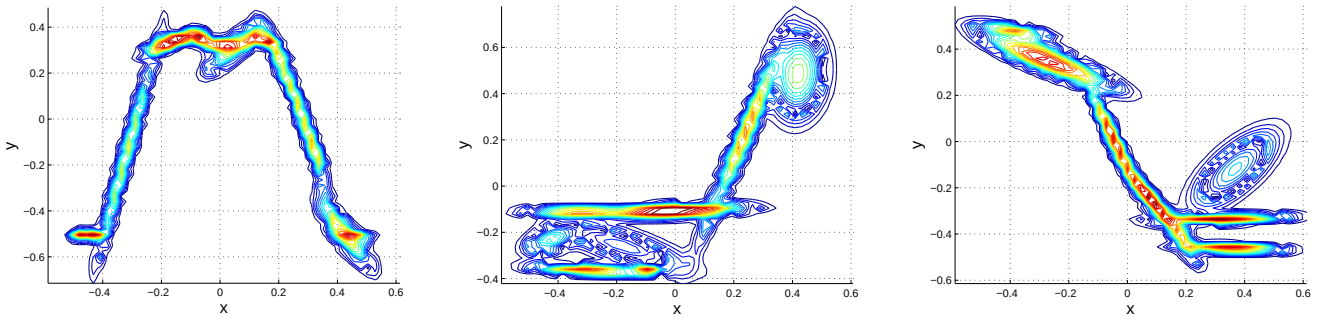

(a) Phase 1 (b) Phase 2 (c) Phase 3

Fig. 8: 2D representation of the learnt models of different phases.

In the experiment, we take another needle driver to hold the needle in place after releasing. In the future, we will use another robot to perform the regrasping task, and therefore the needle posture could be maintained during regrasping. In order to test our robots ability for adapting to needle posture changes, the needle posture was set differently with the posture used in the demonstration, which is orthogonal to the needle driver. These variations are 10mm translation along the grasper, and 20 rotation respectively around the point being grasped. During the experiment, even though the robot posture changed a lot, the needle trajectory is almost same. Most importantly, all tests succeed at one shot without performing redetection. The error in fabric piercing procedure is less 2mm; in each test, the needle almost reach the same entrance and exist point. The experiment shows that the robot can adeptly deal with different needle holding posture and achieve a good accuracy; however, it can only work under a small change of needle orientation (less than 20), which is constrained by the joint limits of the robot. For the purpose of effective using joint range, a weighted Jacobian matrix is used with punishment on the most saturated joints.

Needle regrasping is another important procedure for closing one stitching sequence. In order to sew continuously, the needle gripped by its tip point needs to be passed to another fixed needle driver to change its direction. Thus, using the similar method which we did in fabric piercing part, we demonstrate 3 trajectories for passing needle between two needle drivers. At the start of the demonstration, the needle driver which just finishing fabric piercing takes the needle and feed it into another fixed needle driver. The fixed needle driver grip the middle point of the needle so that the moving needle driver can grip it back at the end point. And then the moving needle driver goes to the initial sewing position and the needle detection is perform for the new sewing cycle. Figure 10 shows the result of this experiment.

IV. Conclusion

References

[1] Donald J Berndt and James Clifford. Using dynamic time warping to find patterns in time series. In *KDD Workshop*, volume 10, pages 359–370. Seattle, WA, 1994.

[2] D.A. Cohn, Z. Ghahramani, and M.I. Jordan. Active learning with statistical models. *Journal of Artificial Intelligence Research*, 4:129–145, 1996.

[3] Srikrishna Iyer, Thomas Looi, and James Drake. A single arm, single camera system for automated suturing. In *Robotics and Automation (ICRA), 2013 IEEE International Conference on*, pages 239–244. IEEE, 2013.

[4] Russell C Jackson and M Cenk Cavusoglu. Needle path planning for autonomous robotic surgical suturing. In *Robotics and Automation (ICRA), 2013 IEEE International Conference on*, pages 1669–1675. IEEE, 2013.

[5] Ankur Kapoor and Russell H Taylor. A constrained optimization approach to virtual fixtures for multi-handed tasks. In *Robotics and Automation, 2008. ICRA 2008. IEEE International Conference on*, pages 3401–3406. IEEE, 2008.

[6] Panagiotis Koustoumpardis, Nikos Aspragathos, and Paraskevi Zacharia. *Intelligent robotic handling of fabrics towards sewing*. INTECH Open Access Publisher, 2006.

[7] Makoto Kudo, Yasuo Nasu, Kazuhisa Mitobe, and Branislav Borovac. Multi-arm robot control system for manipulation of flexible materials in sewing operation. *Mechatronics*, 10(3):371–402, 2000.

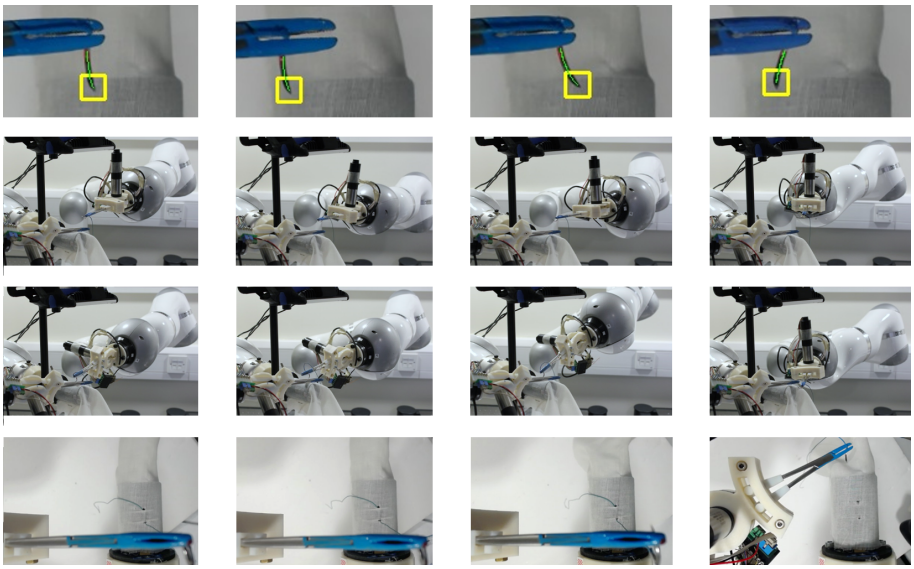

Fig. 9: Qualitative results of the task execution are shown for five different initial needle positions. Detection of the needle in the images is reported in the first row, while the robot adaptation during the task execution is shown in the second and third row. The end of the task is in the last row.

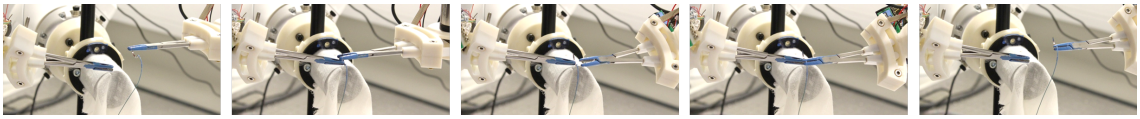

Fig. 10: Sequence of images that shows the automated needle griping between the two needle driver.

[8] Simon Leonard, Kyle L Wu, Yonjae Kim, Alexandra Krieger, and Peter CW Kim. Smart tissue anastomosis robot (star): A vision-guided robotics system for laparoscopic suturing. *Biomedical Engineering, IEEE Transactions on*, 61(4):1305–1317, 2014.

[9] Diego Lo, Paulo RS Mendonça, Andy Hopper, et al. Trip: A low-cost vision-based location system for ubiquitous computing. *Personal and Ubiquitous Computing*, 6(3):206–219, 2002.

[10] Hermann Mayer, Faustino Gomez, Daan Wierstra, Istvan Nagy, Alois Knoll, and Jürgen Schmidhuber. A system for robotic heart surgery that learns to tie knots using recurrent neural networks. *Advanced Robotics*, 22(13-14):1521–1537, 2008.

[11] Florent Nageotte, Philippe Zanne, Michel De Mathelin, and Christophe Doignon. A circular needle path planning method for suturing in laparoscopic surgery. In *Robotics and Automation, 2005. ICRA 2005. Proceedings of the 2005 IEEE International Conference on*, pages 514–519. IEEE, 2005.

[12] Nicolas Padoy and Gregory D Hager. Human-machine collaborative surgery using learned models. In *Robotics and Automation (ICRA), 2011 IEEE International Conference on*, pages 5285–5292. IEEE, 2011.

[13] Johannes Schrimpf, Magnus Bjerkeng, and Geir Mathisen. Velocity coordination and corner matching in a multi-robot sewing cell. In *Intelligent Robots and Systems (IROS 2014), 2014 IEEE/RSJ International Conference on*, pages 4476–4481. IEEE, 2014.

[14] Johannes Schrimpf and Lars Erik Wetterwald. Experiments towards automated sewing with a multi-robot system. In *Robotics and Automation (ICRA), 2012 IEEE International Conference on*, pages 5258–5263. IEEE, 2012.

[15] Johannes Schrimpf, Lars Erik Wetterwald, and Morten Lind. Real-time system integration in a multi-robot sewing cell. In *Intelligent Robots and Systems (IROS), 2012 IEEE/RSJ International Conference on*, pages 2724–2729. IEEE, 2012.

[16] Christoph Staub, Takayuki Osa, Alois Knoll, and Robert Bauernschmitt. Automation of tissue piercing using circular needles and vision guidance for computer aided laparoscopic surgery. In *Robotics and Automation (ICRA), 2010 IEEE International Conference on*, pages 4585–4590. IEEE, 2010.

[17] Jur Van Den Berg, Stephen Miller, Daniel Duckworth, Humphrey Hu, Andrew Wan, Xiao-Yu Fu, Ken Goldberg, and Pieter Abbeel. Superhuman performance of surgical tasks by robots using iterative learning from human-guided demonstrations. In *Robotics and Automation (ICRA), 2010 IEEE International Conference on*, pages 2074–2081. IEEE, 2010.